

PCCP

Accepted Manuscript



This is an *Accepted Manuscript*, which has been through the Royal Society of Chemistry peer review process and has been accepted for publication.

Accepted Manuscripts are published online shortly after acceptance, before technical editing, formatting and proof reading. Using this free service, authors can make their results available to the community, in citable form, before we publish the edited article. We will replace this *Accepted Manuscript* with the edited and formatted *Advance Article* as soon as it is available.

You can find more information about *Accepted Manuscripts* in the [Information for Authors](#).

Please note that technical editing may introduce minor changes to the text and/or graphics, which may alter content. The journal's standard [Terms & Conditions](#) and the [Ethical guidelines](#) still apply. In no event shall the Royal Society of Chemistry be held responsible for any errors or omissions in this *Accepted Manuscript* or any consequences arising from the use of any information it contains.

Cite this: DOI: 10.1039/xxxxxxxxxx

Quasiparticle and excitonic gaps of one-dimensional carbon chains

E. Mostaani,^a B. Monserrat,^{bc} N. D. Drummond,^a and C. J. Lambert^aReceived Date
Accepted Date

DOI: 10.1039/xxxxxxxxxx

www.rsc.org/journalname

We report diffusion quantum Monte Carlo (DMC) calculations of the quasiparticle and excitonic gaps of hydrogen-terminated oligoynes and extended polyynes. The electronic gaps are found to be very sensitive to the atomic structure in these systems. We have therefore optimised the geometry of polyynes by directly minimising the DMC energy with respect to the lattice constant and the Peierls-induced carbon–carbon bond-length alternation. We find the bond-length alternation of polyynes to be 0.136(2) Å and the excitonic and quasiparticle gaps to be 3.30(7) and 3.4(1) eV, respectively. The DMC zone-centre longitudinal optical phonon frequency of polyynes is 2084(5) cm⁻¹, which is consistent with Raman spectroscopic measurements for large oligoynes.

1 Introduction

Carbon is the fourth most abundant element in the universe and is fundamental to life as we know it. Carbon exists in a number of strikingly different forms, including famous examples such as *sp*³-bonded diamond and two-dimensional *sp*²-bonded graphene. A less well-known form of pure carbon is polyyne, which is a one-dimensional (1D) *sp*-bonded chain of carbon atoms with alternating single and triple bonds. The observed presence of carbon chains in interstellar space and circumstellar shells^{1,2} has inspired considerable effort to synthesise polyyne in the laboratory, leading among other things to the discovery of fullerenes³. Recent experiments have shown that it is possible to produce a long linear chain of more than 200 carbon atoms inside a protector such as a double-walled carbon nanotube (DWCNT)⁴ and also to synthesise stable oligoynes (short polyyne molecules) with up to 44 carbon atoms⁵ and a variety of terminal groups^{6–12}. Polyyne is of particular interest as the ideal interconnect in single-molecule nanoelectronic circuitry, including spintronic devices^{13–16}, and has potential applications in nanomechanical devices^{17–19}. Unfortunately, the characterisation of the optical and electronic properties of polyyne continues to present many challenges. Our aim in this work is to address the source of experimental and theoretical discrepancies by establishing the structural and electronic properties of polyyne with quantitative accuracy.

The band gap of polyyne is strongly dependent on the bond-

length alternation (BLA) that arises from the so-called Peierls distortion of the linear carbon chain²⁰. A carbon chain has a half-filled band structure with degenerate π orbitals; therefore a small distortion can reduce the translational symmetry and introduce gaps into the energy bands at or near the Fermi energy, thereby lowering the total energy. Estimating the gap of extended polyyne by extrapolating from the measured absorption spectra of oligoynes has been attempted in several studies^{5,7,10,11,21–23}; however, long oligoynes are needed to minimise the effects of terminal groups, and the interpretation of the absorption spectra of oligoynes is not always straightforward. Most first-principles studies of the electronic structure of polyyne to date are based on density functional theory (DFT) with different exchange–correlation functionals^{24–28}. The local density approximation (LDA) and Perdew–Burke–Ernzerhof²⁹ (PBE) functionals substantially underestimate the gap. Hybrid exchange–correlation functionals such as the Becke (three-parameter) Lee–Yang–Parr^{30,31} (B3LYP) and Heyd–Scuseria–Ernzerhof^{32,33} (HSE06) functionals, which include a fraction of exact exchange, perform significantly better, but the predicted gaps still underestimate the range of gaps indicated by experiment^{5,7,10,11,21–23,34}. On the other hand, Hartree–Fock (HF) theory significantly overestimates gaps. Post-HF quantum-chemistry methods such as Møller–Plesset second-order perturbation theory (MP2) and coupled-cluster singles and doubles with perturbative triples [CCSD(T)] offer a different and potentially far more accurate theoretical approach³⁵; however the gap of polyyne has to be obtained by extrapolating the gaps of small, hydrogen-terminated oligoynes to infinite chain length, introducing significant uncertainty into the results. Previous theoretical studies have reported the BLA of polyyne based on HF^{25,35}, nonhybrid DFT^{25,35}, hybrid DFT²⁵, MP2^{25,35,36}, and CCSD(T)^{35,37} calculations. However, there is

^a Department of Physics, Lancaster University, Lancaster LA1 4YB, United Kingdom. E-mail: e.mostaani@lancaster.ac.uk

^b TCM Group, Cavendish Laboratory, University of Cambridge, 19 J. J. Thomson Avenue, Cambridge CB3 0HE, United Kingdom.

^c Department of Physics and Astronomy, Rutgers University, Piscataway, New Jersey, 08854-8019, USA.

no consensus over either the BLA or the band gap of polyynes in the literature^{38,39}.

In this work, we use highly accurate quantum Monte Carlo (QMC) methods^{40,41} to calculate ground-state and excited-state total energies of isolated hydrogen-terminated oligoynes ($C_{2n}H_2$) and supercells of polyynes subject to periodic boundary conditions. The structure of polyynes is defined by just two parameters, the lattice constant and the BLA, enabling us to carry out a brute-force optimisation of the structure by minimising the QMC total energy. To the best of our knowledge this is the first QMC study of polyynes. We compare our data with experimental and theoretical results in the literature.

The rest of this paper is organised in three sections: in Sec. 2 we describe the computational methodology. Section 3 contains our DFT and QMC results for the BLA and electronic gaps of oligoynes and extended polyynes, including the vibrational renormalisation. Finally, we present our conclusions in Sec. 4.

2 Computational methodology

2.1 DFT calculations

Our DFT calculations were performed using the CASTEP plane-wave-basis code⁴². We relaxed the geometries of hydrogen-terminated oligoynes consisting of up to twelve pairs of carbon atoms using DFT-PBE and DFT-HSE06, and we relaxed the geometry of extended polyynes using DFT-HSE06. The widths and heights of our periodic unit cells were fixed at 20 Bohr radii and, for oligoynes, the length was varied so that a constant amount of vacuum (20 Bohr radii) was maintained between images of the molecule. In our DFT calculations for polyynes we used a grid of 30 k points. We used ultrasoft pseudopotentials in our DFT-PBE calculations and norm-conserving pseudopotentials in our DFT-HSE06 calculations. The plane-wave cutoff energy in our DFT geometry optimisations was 25 Ha.

The DFT-PBE zero-point energy and the DFT-LDA and DFT-PBE phonon dispersion curves of polyynes were obtained using density functional perturbation theory in a primitive cell with 100 k points in the Brillouin zone for both the electronic calculation and the phonon calculation. The DFT-HSE06 zero-point energy and phonon dispersion curve of polyynes were calculated using 32 primitive-cell k points and the method of finite displacements in supercells of up to 16 primitive cells.

2.2 QMC calculations

For our QMC calculations we used the static-nucleus variational and diffusion quantum Monte Carlo (VMC and DMC) methods implemented in the CASINO code⁴³. The DMC method has previously been used to study the excitation energies of a variety of molecules and solids^{44–48}. The many-body trial wave function was composed of Slater determinants multiplied by a Jastrow correlation factor⁴¹. We used DFT-PBE orbitals, which were generated by CASTEP using a plane-wave cutoff energy of 120 Ha, and we used Dirac–Fock pseudopotentials^{49,50}. The plane-wave orbitals were re-represented in a blip (B-spline) basis before they were used in the QMC calculations⁵¹, allowing the use of aperiodic (for oligoynes) and 1D periodic (for polyynes) boundary con-

ditions in our QMC calculations.

For each oligoynes the DFT highest occupied molecular orbital (HOMO) and HOMO–1 are degenerate, as are the lowest unoccupied molecular orbital (LUMO) and LUMO+1. We have therefore studied the effect of multideterminant (MD) Slater–Jastrow trial wave functions for excited, cationic, and anionic states of oligoynes with 4, 6, 8, 10, and 24 carbon atoms as well as a supercell of polyynes composed of 8 primitive cells. The Slater determinants in the MD wave functions contained all the orbital occupancies that are degenerate at the single-particle level. In Table 1 we specify the occupancy of the orbitals in the determinants used in our trial wave functions. We used linear-least-squares energy minimisation^{52–54} and unweighted variance minimisation^{55,56} to optimise the MD coefficients and the Jastrow factor, respectively. Using variance minimisation rather than energy minimisation for the Jastrow factor improves the stability. A test for C_4H_2 showed that the effects of additional determinants containing promotions to the LUMO+2 are negligible.

The DMC energy was linearly extrapolated to zero time step and we verified that finite-population errors in our results are negligible. Fermionic antisymmetry in DMC is imposed by the fixed-node approximation⁵⁷, in which the nodal surface is pinned at that of the trial wave function. The fixed-node approximation allows us to study excited states by using trial wave functions with the appropriate nodal topology. Because the Jastrow factor is strictly positive, the nodal topology is purely determined by the Slater determinants.

Twist-averaging is less important in 1D systems than two- or three-dimensional systems; for example momentum quantisation in a 1D homogeneous electron gas simply introduces a smooth, $O(n^{-2})$ error in the energy per particle⁵⁸.

2.3 DMC quasiparticle and excitonic gaps

A crucial quantity that characterises the electronic structure of polyynes is the quasiparticle gap, which is the difference between the electron affinity and the first ionisation potential. The quasiparticle gap is the energy required to create an unbound electron–hole pair. Within the DMC method quasiparticle gaps are evaluated as

$$\Delta_{qp} = E_I - E_A = E_+ + E_- - 2E_0, \quad (1)$$

where $E_A = E_0 - E_+$ and $E_I = E_- - E_0$ are the electron affinity and ionisation potential, respectively. E_+ and E_- are the total energies of the system with one more electron and one fewer electron, respectively, than the neutral ground state and E_0 is the ground-state total energy. For each oligoynes we separately relaxed the geometries of the neutral ground state, the cation, and the anion using DFT-HSE06 before evaluating the DMC ionisation potential and electron affinity and hence quasiparticle gap, i.e., we use the adiabatic definition of the quasiparticle gap. For polyynes, where there are just two structural parameters, we relaxed the ground-state geometry using DMC, and then used that geometry to obtain the vertical quasiparticle gap; it was verified that the difference between the vertical and adiabatic quasiparticle gaps is small for large oligoynes (see Sec. 3.3).

Table 1 Number of MD terms and orbital occupancies in each determinant for the neutral ground state, singlet and triplet excited states, cationic state, and anionic state in each of our calculations. “H” and “L” denote the HOMO and LUMO, respectively. Note that the HOMO and HOMO−1 orbitals are degenerate, as are the LUMO and LUMO+1 orbitals. All orbitals up to the HOMO−2 are occupied in each determinant.

State	No. determinants	Orbital occupancy							
		Spin-up				Spin-down			
		H−1	H	L	L+1	H−1	H	L	L+1
Neutral ground state	1	•	•			•	•		
Singlet excited state	8	•		•		•	•		
			•	•		•	•		
		•			•	•	•		
		•	•			•	•	•	
		•	•			•	•		•
		•	•			•	•		•
		•	•			•	•		•
		•	•			•	•		•
Triplet excited state	4	•				•	•	•	
		•		•		•	•	•	
			•			•	•	•	
			•			•	•	•	
Cationic state	2	•				•	•		
		•				•	•		
Anionic state	2	•	•	•		•	•		
		•	•		•	•	•		

Excitonic gaps are evaluated as

$$\Delta_{\text{exc}} = E_{\text{pr}} - E_0, \quad (2)$$

where E_{pr} is the DMC total energy when a single electron is promoted from the valence-band maximum to the conduction-band minimum (without changing its spin for a singlet excitonic gap; swapping its spin for a triplet excitonic gap). In the ground-state geometry, the singlet excitonic gap is equivalent to the vertical optical absorption gap, i.e., the energy at which the onset of photoabsorption occurs. The DMC static-nucleus excitonic gaps are corrected using the DFT vibrational renormalisation method described in Sec. 2.5.

The excitonic gaps are smaller than the quasiparticle gap due to the attraction between the excited electron and the hole left in the valence band. The exciton binding energy is the difference between the quasiparticle gap and the excitonic gap. Fixed-node errors in the DMC total energies are always positive and are expected to cancel to a significant extent when energy gaps are calculated.

2.4 Finite-size effects

The BLA of polyne in the ground state was evaluated for three supercells consisting of 8, 12, and 16 primitive unit cells. To remove finite-size effects in the energy we fitted

$$E(n) = E(\infty) + An^{-2}, \quad (3)$$

where $E(\infty)$ and A are fitting parameters, to our DMC ground-state energies per primitive cell $E(n)$ in supercells of n primitive cells⁵⁸.

The DMC quasiparticle and excitonic gaps $\Delta(n)$ of polyne were calculated for supercells of $n = 8, 10, 12,$ and 16 primitive cells, and then extrapolated to infinite length by fitting

$$\Delta(n) = \Delta(\infty) + Bn^{-1} \quad (4)$$

to the data, where $\Delta(\infty)$ and B are fitting parameters. When a single particle is added to a finite simulation cell subject to periodic boundary conditions, a periodic lattice of quasiparticles is formed. The energy of this unwanted lattice of quasiparticles goes as the Madelung constant of the supercell lattice and results in a significant finite-size error in the electron affinity and ionisation potential. The 1D Madelung energy in Hartree atomic units ($\hbar = m_e = |e| = 4\pi\epsilon_0 = 1$) is given by $v_M = [-0.2319 - 2\log(an)]/(an)$, where a is the lattice constant and n is the number of primitive cells. Ignoring the logarithmic terms, the Madelung constant falls off as the reciprocal of the linear size of the supercell, i.e., as $1/n$. Additional finite-size effects in the exciton energy arise from the fact that the energy is evaluated using the Ewald interaction rather than $1/r$. However, by calculating the ground-state energy of an exciton modelled by a single electron and a single hole moving strictly in 1D in a periodic cell as a function of cell length (Fig. 1), we find that these finite-size errors fall off more rapidly, as $1/n^3$. Equation (4) is therefore an appropriate fitting function for extrapolating gaps to the thermodynamic limit. The finite-size error in the quasiparticle gap is significantly larger than the finite-size error in the excitonic gap, because we do not change the number of electrons in the simulation cell when calculating the latter. The Madelung constant is negative, and hence the finite-size error in the quasiparticle gap is large and negative, resulting in a negative exciton binding energy at finite system size. Physically this is caused by the fact that, when a charged particle is added to or removed from a finite, periodic cell in which particles interact via the Ewald potential, a neutralising background is implicitly introduced. This neutralising background charge density vanishes in the infinite-system limit, and hence our quasiparticle gaps are only physically meaningful in the infinite-system limit. For a finite molecule, by contrast, the $1/r$ Coulomb interaction is used, and hence no additional neutralising background is introduced when a charged particle is added to or removed from a neutral molecule.

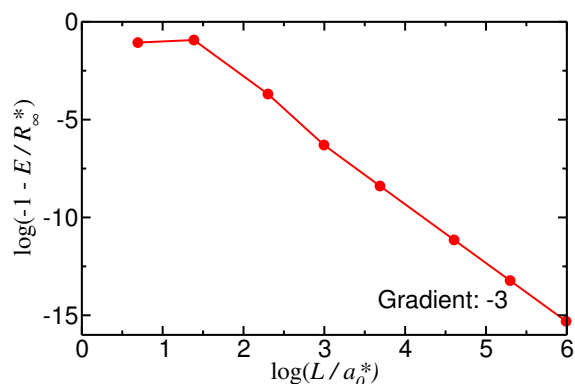


Fig. 1 Finite-size error in the total energy of a 1D exciton against the periodic cell length $L = an$, where a is the lattice constant and n is the number of primitive cells. $R_\infty^* = \mu/2$ is the exciton Rydberg and $a_0^* = 1/\mu$ is the exciton Bohr radius. $\mu = m_e m_h / (m_e + m_h)$ is the reduced mass of the electron–hole pair.

2.5 Vibrational renormalisation

Our DMC energies have been obtained in the static-nucleus approximation. We have used DFT methods to determine vibrational corrections to our DMC results by including phonon zero-point energies in our reported atomisation energies and by averaging vertical DFT excitonic gaps over phonon displacements in the ground-state geometry to obtain a vibrational correction to the excitonic gap.

Vibrational renormalisations to electronic band gaps have recently been shown to be as large as -0.5 eV for diamond^{59–61} and diamondoids⁶². We have therefore investigated the effects of electron–phonon coupling on the gaps of carbon chains.

The vibrational renormalisations to the excitonic gaps were calculated at the DFT level with the same parameters as those used for the static calculations. Harmonic vibrational frequencies and eigenvectors were determined using the finite-displacement method⁶³. The resulting harmonic vibrational wave functions were used to calculate vibrational expectation values of the gaps according to

$$\langle \Delta_{\text{exc}} \rangle = \langle \Phi(\mathbf{q}) | \Delta_{\text{exc}}(\mathbf{q}) | \Phi(\mathbf{q}) \rangle, \quad (5)$$

where $|\Phi\rangle$ is the harmonic vibrational wave function and \mathbf{q} is a vector containing the amplitudes of the normal modes of vibration, which therefore labels atomic configurations. A Monte Carlo sampling technique^{62,64} was used to evaluate Eq. (5). For oligynes, a quadratic approximation to Eq. (5) was also employed⁶⁵, yielding results consistent with those obtained using Monte Carlo.

2.6 Test of our method: benzene molecule

DMC has proven to be a highly accurate method for calculating excitation energies within the static-nucleus approximation^{44–48}. However, as a brief test of our methodology, we have calculated the static-nucleus DMC ionisation potential and singlet and triplet optical-absorption (excitonic) gaps of a benzene molecule in vacuum. The geometry was relaxed in both the neutral ground state and the cationic state using DFT-PBE. The resulting adiabatic DMC ionisation potential is 9.24(2) eV, which is in ex-

cellent agreement with the experimental value of 9.24384(6) eV obtained by the zero kinetic energy (ZEKE) photoelectron spectroscopy method⁶⁶. If the ground-state geometry is used for both the ground state and the cation (i.e., the vertical ionisation potential is calculated) then the static-nucleus DMC ionisation potential is 9.39(3) eV. This illustrates that, when calculating ionisation potentials and electron affinities (and hence quasiparticle gaps) for small molecules, it can be important to relax the geometry in the neutral, cationic, and anionic states.

Static-nucleus DMC predicts the singlet and triplet excitonic gaps of benzene to be 5.63(4) and 4.56(4) eV, respectively, which are about 0.7 eV larger than the experimental values of 4.9 eV⁶⁷ and 3.9 eV⁶⁸, respectively. This difference is largely due to the neglect of vibrational effects.

In Fig. 2 we report gap-renormalisation results for benzene, where we have relaxed the benzene molecule and calculated the band gap using DFT-PBE. The static HOMO–LUMO gap is 5.106 eV, and it reduces to 4.653 eV when the effects of quantum mechanical zero-point motion are included. This gives a zero-point correction to the band gap of -0.453 eV. Using the DFT-PBE geometry, DFT-HSE06 predicts a static band gap of 6.160 eV, which is larger than the DFT-PBE band gap, as expected, and a renormalised band gap of 5.660 eV, with a zero-point correction of -0.500 eV. Similar results are obtained if the benzene molecule is relaxed using DFT-HSE06 instead of DFT-PBE. We note that small changes in these results could arise if the renormalisation were calculated for the full optical absorption spectrum rather than individual electronic eigenvalues⁶⁹.

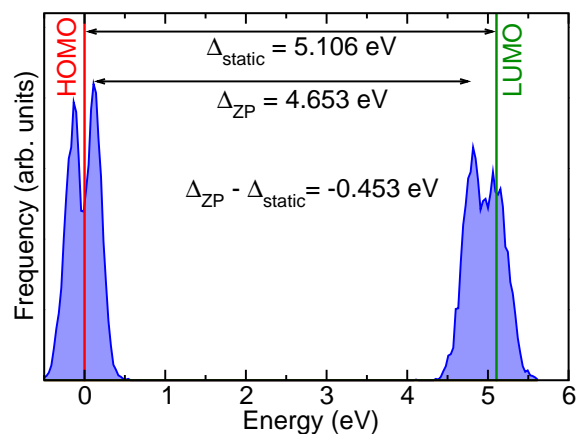


Fig. 2 Distribution of HOMO and LUMO DFT-PBE eigenvalues of benzene at the static-lattice level (vertical red and green lines) and including the effects of zero-point motion (shaded blue curves).

In summary, the DFT vibrational renormalisation of the excitonic gap of benzene ranges from -0.45 eV to -0.50 eV, depending on the choice of exchange–correlation functional. This correction enormously improves the agreement between theory and experiment, as previously observed in diamondoids⁵⁹. This indicates that we can expect our vibrationally renormalised DMC gaps to be accurate to within 0.2–0.3 eV.

3 Results and discussion

3.1 Atomic structures and atomisation energies of linear hydrogen-terminated oligoynes

The ground-state BLAs at the centres of oligoynes have previously been calculated using a variety of theoretical methods^{27,37,70,71}; some of the results are compared with our DMC and DFT data in Fig. 3. The PBE functional completely fails to describe the BLA for long chains, while spin-restricted HF theory predicts a very large BLA. Our DFT-HSE06 BLAs are in agreement with the values previously obtained using the B3LYP functional^{27,70}, and are close to the MP2 results wherever the latter are available⁷¹; however none of these BLA curves tends to the DMC BLA of polyyne as the chain length increases. By contrast, the CCSD(T) BLAs³⁷ of oligoynes appear to tend to a limit only slightly less than the DMC result for polyyne. Our DMC results for the BLA of extended polyyne provide benchmark data with which the results of other theories may be compared.

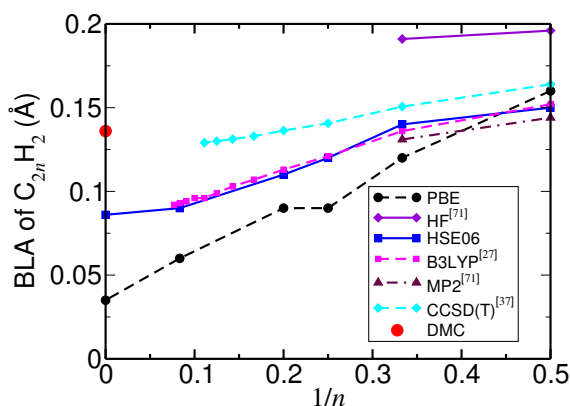


Fig. 3 Optimised BLA at the centre of a hydrogen-terminated oligoyne in the ground state against the reciprocal of the number n of pairs of carbon atoms.

The DMC static-nucleus atomisation energy of the oligoyne $C_{2n}H_2$ is defined as $2n$ times the DMC total energy of an isolated, spin-polarised carbon atom plus two times the DMC total energy of an isolated hydrogen atom minus the DMC static-nucleus total energy of $C_{2n}H_2$. The DMC atomisation energies of oligoynes obtained using geometries relaxed in DFT-HSE06 and DFT-PBE calculations are compared in Fig. 4. For oligoynes consisting of up to five pairs of carbon atoms, the difference between the DMC atomisation energies with the DFT-PBE and DFT-HSE06 geometries is negligible.

3.2 Atomic structure, vibrational properties and atomisation energy of polyyne

As the number of carbon atoms goes to infinity, the effects of the terminal groups become negligible; therefore polyyne can be considered to be a 1D periodic chain with a primitive cell composed of two carbon atoms with alternating triple and single bonds.

In order to obtain the BLA of an infinite chain, we considered supercells subject to periodic boundary conditions, in which the lattice constant was fixed at the DFT-BLYP²⁵ value of 2.58 Å. We calculated DMC energies at different BLAs ranging from 0.09 to

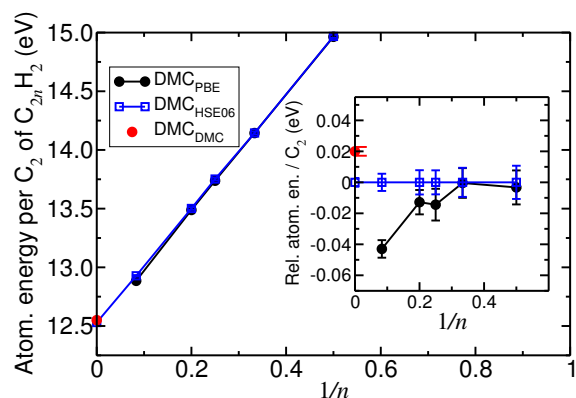


Fig. 4 Static-nucleus DMC atomisation energies of hydrogen-terminated oligoynes as a function of the reciprocal of the number n of pairs of carbon atoms. “DMC_x” indicates a DMC atomisation energy calculated using the geometry optimised by method X. The inset shows the relative atomisation energies of hydrogen-terminated oligoynes as a function of the reciprocal of the number n of pairs of carbon atoms.

0.18 Å and fitted a quadratic to our DMC data, as shown in Fig. 5(a), to locate the minimum.

The DMC energy minima of supercells consisting of 8, 12, and 16 primitive cells are at BLAs of 0.152(5), 0.145(2), and 0.144(1) Å, respectively. When the BLA is 0.15 Å, the C≡C triple-bond length is 1.215 Å and the ratio of the C≡C triple-bond length to the lattice constant is 0.471. We then computed the ground-state DMC energy of polyyne at several lattice constants, from 2.4 to 2.7 Å, holding the ratio of the C≡C bond length to the lattice constant at 0.471 for the supercell composed of 8 primitive cells and holding the C≡C bond length at 1.215 Å for the supercell consisting of 16 primitive cells. The quadratic fits to the DMC data in the inset of Fig. 5(a) are in good agreement, and the ground-state energy is minimised at lattice constants of 2.5817(9) Å and 2.5822(5) Å for supercells of 8 and 16 primitive cells, respectively. Finally, the DMC energy was calculated at lattice constant 2.5817 Å for different BLAs as shown in Fig. 5(b) together with quadratic fits. The DMC energy minima for supercells consisting of 8 and 16 primitive cells occur at BLAs of 0.142(2) and 0.136(2) Å, respectively, which are in reasonable agreement. Furthermore, the BLA obtained in a supercell of 16 primitive cells does not differ significantly from the BLA 0.133(2) Å obtained by minimising the DMC energy extrapolated to infinite system size using Eq. (3). We therefore report the BLA obtained in a supercell of 16 primitive cells [0.136(2) Å] as our final result.

The DMC data shown in Fig. 5 for the ground-state energy per primitive cell $e(b)$ against BLA b can be used to calculate the longitudinal optical (LO) phonon frequency of polyyne at Γ . Near the minimum of the energy we may write

$$e(b) = e_0 + \frac{1}{2} \frac{m_C}{2} \omega^2 \left(\frac{b}{2} - \frac{b_0}{2} \right)^2, \quad (6)$$

where b is the bond-length alternation, b_0 and e_0 are constants, $m_C/2$ is the reduced mass of the two carbon atoms in polyyne’s primitive unit cell, and ω is the LO phonon frequency at Γ . In

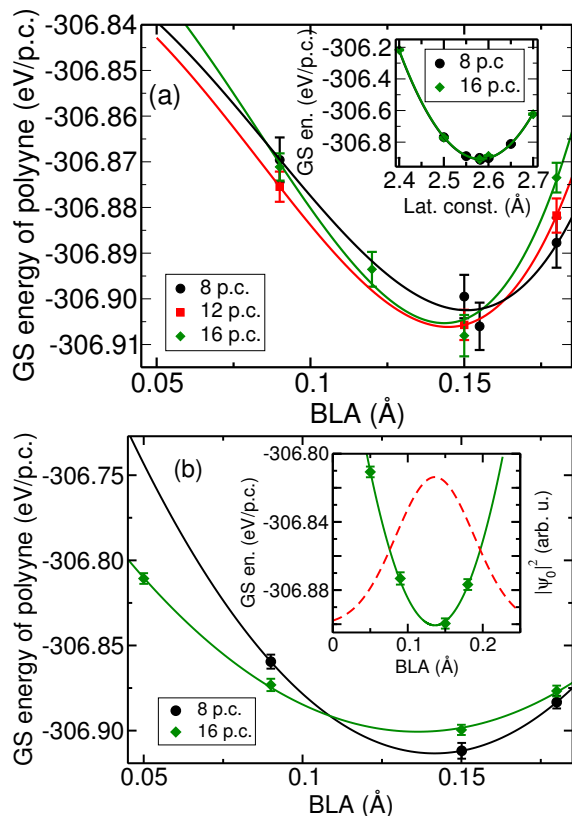


Fig. 5 (a) Ground-state (GS) DMC energy of polyynes as a function of BLA for lattice constant 2.58 Å in different sizes of simulation supercell. The inset shows the ground-state DMC energy of polyynes against the lattice constant at a fixed ratio of C=C bond length to lattice constant for 8 primitive cells (p.c.) and a fixed C≡C bond length for 16 primitive cells. (b) GS DMC energy of polyynes as a function of BLA for lattice constant 2.5817 Å in different sizes of supercell. The minimum of the DMC energy, $-306.901(3)$ eV per primitive cell, is at BLA $b_0 = 0.136(2)$ Å. The inset shows the square modulus $|\psi_0|^2$ of the longitudinal optical phonon ground-state wave function for a supercell composed of 16 primitive cells as a function of BLA.

terms of the BLA b , the ground-state wave function of the zone-centre LO phonon mode of polyynes in Hartree atomic units is

$$\psi_0(b) = \left(\frac{m_C \omega}{2\pi}\right)^{1/4} \exp\left[-\frac{m_C \omega}{2} \left(\frac{b}{2} - \frac{b_0}{2}\right)^2\right]. \quad (7)$$

Fitting Eq. (6) to the static-nucleus DMC energy of a supercell composed of 16 primitive cells of polyynes gives $\omega = 2084(5)$ cm^{-1} . The standard deviation of b in the ground state is $\sigma_b = \sqrt{2/(m_C \omega)} = 0.052$ Å. The square modulus of the LO phonon ground-state wave function is plotted in the inset of Fig. 5(b).

In Fig. 6 we show the DFT-LDA, DFT-PBE, and DFT-HSE06 phonon dispersion curves of polyynes. Our DFT-PBE phonon dispersion curve is in good agreement with previous DFT-PBE results in the literature⁷². The DMC LO phonon frequency at Γ is $2084(5)$ cm^{-1} , which is significantly higher than the frequencies of 1162, 1223, 1723, 1844, and ~ 1970 cm^{-1} obtained using DFT-LDA, DFT-PBE, DFT-HSE06, DFT-B3LYP⁷³, and equally-scaled spin components MP2⁷⁴, respectively. It is clear that DFT provides a poor description of both the Peierls distortion and the related LO phonon

behaviour. The LO phonon frequencies of oligynes with up to 40 carbon atoms have been measured by Raman spectroscopy to be in the region of 1900–2300 cm^{-1} ; the precise value depends on the terminal groups, solvent, and the number of carbon atoms in the chain⁷⁵.

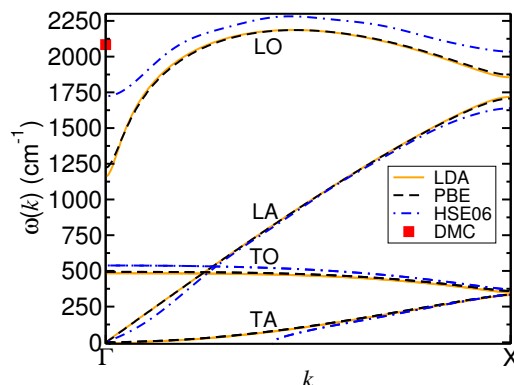


Fig. 6 Phonon dispersion curve of polyynes calculated using DFT-LDA, DFT-PBE, and DFT-HSE06. The DMC LO frequency at Γ is shown by the red square. “T,” “L,” “A,” and “O” stand for transverse, longitudinal, acoustic, and optical, respectively. We believe the slight instability of the TA branch in the DFT-HSE06 dispersion curve is a numerical artifact.

To evaluate the quasiparticle gap of polyynes, the atomic structure should be in principle be relaxed when an electron is added to or removed from a supercell. Although the effect on the structure becomes vanishingly small as the supercell becomes large [falling off as $O(n^{-1})$, where n is the number of primitive cells in the supercell], the effect on the gap remains finite, because the gap is a difference of total energies, which increase as $O(n)$ with supercell size and depend on the atomic structure. However, the re-optimisation of the geometry at each system size adds noise that affects the extrapolation to the limit of infinite system size and, as shown in Fig. 9, the effect of relaxing the geometries of cations and anions on the quasiparticle gap (i.e., the difference between the vertical and adiabatic quasiparticle gaps) is small for large oligynes.

In Table 2 we compare the equilibrium BLAs and lattice constants of polyynes obtained using different methods. DFT-LDA, PBE, and HSE06 underestimates the BLA of polyynes, while HF theory predicts a larger BLA than DMC. The DMC BLA happens to be in agreement with the Becke-half-and-half-Lee-Yang-Parr (BHHLYP) and Kang-Musgrave-Lee-Yang-Parr (KM-LYP) results²⁵. The BLA of extended polyynes within a DWCNT has been measured to be 0.1 Å⁴, which we expect to be different from our results for free-standing polyynes due to the effects of charge transfer between the polyynes and the DWCNT.

In Fig. 7 we compare the ground-state DMC energy of polyynes calculated using BLAs obtained by DMC and DFT-HSE06 as a function of system size. To reduce finite-size errors, we considered supercells consisting of 8, 12, and 16 primitive cells, with the BLA and lattice constant fixed as a function of cell size, and we fitted a curve of the form Eq. (3). The extrapolated DMC energies with the DFT-HSE06 and DMC geometries are $-306.875(2)$ and $-306.895(2)$ eV per primitive cell, respectively, confirming that

Table 2 BLA and lattice constant a of polyynes as calculated or measured by different methods. r_1 and r_2 are the C–C and C≡C bond lengths, respectively. “PBC” indicates that periodic boundary conditions were used; otherwise results were obtained by extrapolation from a series of oligoynes. Where known, the number n of pairs of carbon atoms in the longest chain for which calculations were performed is given. Where a citation is not given in the table, the data were obtained in the present work. The experimental result is for polyynes encapsulated in a DWCNT.

Method	n	a (Å)	r_1 (Å)	r_2 (Å)	BLA (Å)
DFT-LDA ²⁵	PBC	2.566	1.297	1.269	0.028
DFT-LDA ³⁵	PBC	2.532	1.286	1.246	0.040
DFT-PBE	PBC	2.565	1.300	1.265	0.035
DFT-PBE1PBE ²⁵	36				0.093
DFT-HSE06	PBC	2.56	1.323	1.237	0.086
DFT-KMLYP ²⁵	36				0.135
DFT-BHLYP ²⁵	36				0.134
DFT-B3LYP ²⁵	36				0.088
DFT-O3LYP ²⁵	36				0.067
DFT-BLYP ²⁵	PBC	2.582	1.309	1.273	0.036
HF ²⁵	36				0.183
MP2 ²⁵	20				0.060
MP2 ³⁵		2.554	1.337	1.217	0.120
MP2/CO ³⁶		2.6	1.346	1.254	0.092
CCSD ³⁵		2.559	1.362	1.197	0.165
CCSD(T) ³⁵		2.565	1.358	1.207	0.151
CCSD(T) ³⁷	9	2.586	1.357	1.229	0.128
DMC	PBC	2.5817(9)	1.359(2)	1.223(2)	0.136(2)
Exp. in DWCNT ⁴	~ 200	2.558	1.329	1.229	0.100

DMC is needed for geometry optimisation.

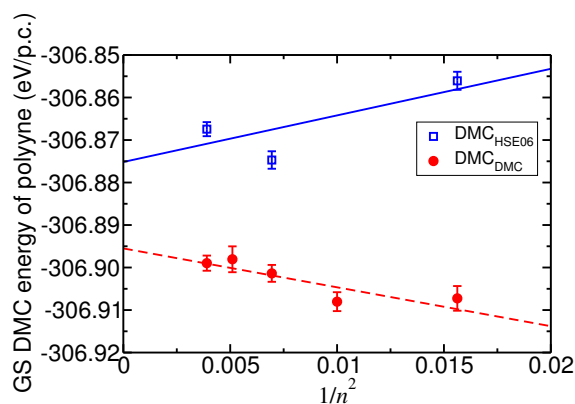


Fig. 7 Ground-state DMC energy of polyynes against the reciprocal of the square of the number n of primitive cells (p.c.) in the supercell. “DMC_X” indicates a DMC energy calculated using the geometry optimised by method X.

DMC atomisation energies of extended polyynes obtained using DMC and DFT-HSE06 geometries are compared in Table 3. The DMC static-nucleus atomisation energy with the DMC geometry is 12.55(1) eV, which is outside the range 10.7–11.4 eV estimated by MP2, CCSD, and CCSD(T) methods in Ref. 35; however the latter were calculated by extrapolating results obtained for hydrogen-terminated oligoynes of up to eight pairs of carbon atoms to infinite chain length, whereas our polyynes calculations use periodic boundary conditions. DFT phonon zero-point energies are reported in the caption of Table 3. As shown in Fig. 4, the difference between DMC atomisation energies with DFT-PBE and DFT-HSE06 geometries is negligible for small oligoynes.

Table 3 Static-nucleus atomisation energy E_c of polyynes as obtained by different methods. “DMC_{DMC}” and “DMC_{HSE06}” indicate that the DMC energy of polyynes was calculated using the DMC- and DFT-HSE06-optimised geometries, respectively. (The DFT-PBE and DFT-HSE06 phonon zero-point energies of polyynes are 0.260 and 0.264 eV, respectively. The zero-point energy is a correction that should be subtracted from the atomisation energy before comparison with experiment.)

Method	E_c (eV)
DFT-PBE	13.71
DFT-HSE06	12.47
MP2 ³⁵	11.375
CCSD ³⁵	10.678
CCSD(T) ³⁵	11.053
DMC _{HSE06}	12.53(1)
DMC _{DMC}	12.55(1)

3.3 Quasiparticle and excitonic gaps of hydrogen-terminated oligoynes

The DFT-HSE06 band structure of polyynes is shown in Fig. 13. Polyynes is a semiconductor with a direct band gap at the X point of the Brillouin zone, as expected on the basis of the Peierls distortion mechanism.

Figure 8(a) shows that using an MD trial wave function reduces the DMC singlet and triplet excitonic gaps of small oligoynes (by up to 1.3 eV for C_4H_2). The reduction in singlet gaps is larger than the reduction in triplet gaps. However, Fig. 8(b) shows that using an MD wave function does not significantly affect the quasiparticle gaps of oligoynes apart from C_4H_2 . As the length of the molecule increases, the effects of using multiple determinants on the excitonic gaps decreases, becoming negligible for polyynes.

The DMC quasiparticle gaps of oligoynes are compared with other theoretical results in Fig. 9. The HF method overestimates the quasiparticle gap, while DFT with various functionals considerably underestimates the gap. The DMC quasiparticle gaps calculated using DFT-HSE06 and DFT-PBE geometries are in agreement for oligoynes consisting of fewer than ten carbon atoms, but gradually start to differ from each other for longer oligoynes, with the difference in the DMC gaps reaching 0.8(1) eV for $C_{24}H_2$. This demonstrates that, not only the method used to calculate the gap, but also the method used to optimise the geometry of polyynes must be highly accurate. Using the ground-state geometry rather than separately optimised geometries for the ground, cationic, and anionic states increases the quasiparticle gap by less than 0.15 eV for oligoynes longer than C_8H_2 (i.e., the difference between the vertical and the adiabatic quasiparticle gap is negligible for large oligoynes). The DMC quasiparticle gap of polyynes, evaluated using the DMC ground-state geometry, is 3.6(1) eV.

We plot the static-nucleus singlet and triplet excitonic gaps of different oligoynes in Fig. 10(a). Singlet–triplet splitting (the difference of singlet and triplet excitonic gaps) against the reciprocal of the number n of pairs of carbon atoms in oligoynes is small, about 0.1–0.2 eV as shown in Fig. 10(b). Using DFT-HSE06 geometries instead of DFT-PBE geometries typically increases the DMC gaps by around 0.2 eV for small oligoynes. The DMC singlet and triplet excitonic gaps of extended polyynes using the ground-state DMC geometry are obtained by extrapolating results ob-

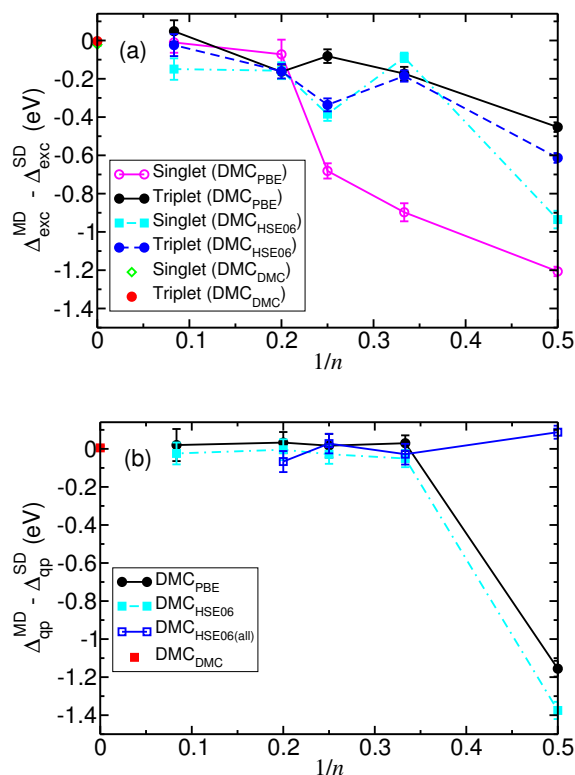


Fig. 8 (a) Difference ($\Delta_{\text{exc}}^{\text{MD}} - \Delta_{\text{exc}}^{\text{SD}}$) of the DMC excitonic gaps of oligynes obtained using MD and single-determinant Slater–Jastrow trial wave functions as a function of the reciprocal of the number n of pairs of carbon atoms. (b) Difference ($\Delta_{\text{qp}}^{\text{MD}} - \Delta_{\text{qp}}^{\text{SD}}$) of the DMC quasiparticle gaps of oligynes obtained using MD and single-determinant Slater–Jastrow trial wave functions as a function of the reciprocal of the number n of pairs of carbon atoms. DMC_X indicates a DMC gap calculated using the geometry optimised by method X. “X(all)” in the subscript indicates the use of geometries separately optimised using method X for the neutral ground state, cationic state, and anionic state.

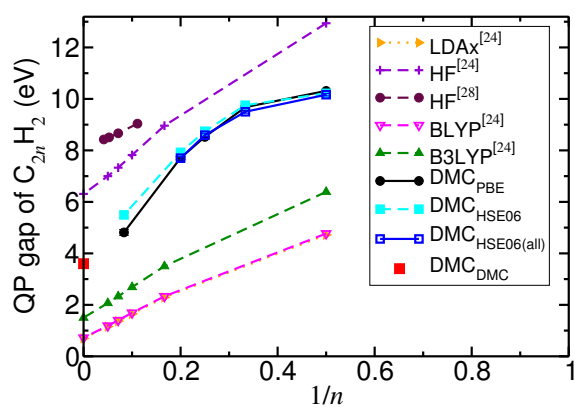


Fig. 9 Static-nucleus quasiparticle (QP) gaps of hydrogen-terminated oligynes against the reciprocal of the number n of pairs of carbon atoms. “DMC_{PBE}” and “DMC_{HSE06}” denote DMC gaps calculated using DFT-PBE and DFT-HSE06 ground-state geometries, respectively. “DMC_{X(all)}” denotes DMC quasiparticle gaps calculated using geometries optimised by method X separately for the neutral ground state, cationic state, and anionic state.

tained in finite, periodic cells to infinite system size, as discussed in Sec. 3.4.

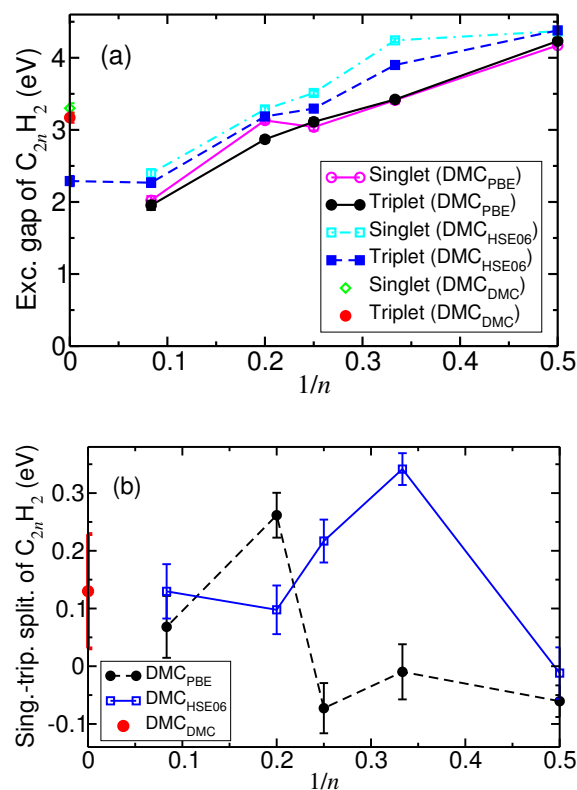


Fig. 10 (a) DMC static-nucleus singlet and triplet excitonic gaps for oligynes, whose geometries are optimised by DFT-PBE and DFT-HSE06, against the reciprocal of the number n of pairs of carbon atoms. DMC_X indicates a DMC gap calculated using the geometry optimised by method X. (b) DMC singlet–triplet splitting for oligynes obtained with DFT-PBE and DFT-HSE06 geometries. The polyyne limit was obtained using the DMC geometry.

In Fig. 11 we show zero-point corrections to the excitonic gaps of hydrogen-terminated oligynes. The error bars in the Monte Carlo results indicate the statistical uncertainty arising from the Monte Carlo integration. The band-gap corrections calculated using the quadratic method are in good agreement with the Monte Carlo results. In the quadratic method, the coupling of each vibrational normal mode to the electronic band extrema is treated individually, hence providing access to the microscopic behaviour of the system. Within DFT-PBE, the largest phonon zero-point correction to the gap is found in the shortest oligoyne considered, C_4H_2 , at about -0.14 eV. The correction decreases with increasing chain length to about -0.05 eV for C_{24}H_2 . The decrease in the strength of electron–phonon coupling with increasing chain size in oligynes can be attributed to the decrease in the importance of the hydrogen atoms at the terminations. The DFT-HSE06 zero-point correction to the excitonic gap of polyyne is obtained by extrapolation to infinite system size as explained in Sec. 3.4. Phonon renormalisation of gaps is clearly not as important in oligynes as in either benzene or diamond.

3.4 Quasiparticle and excitonic gaps of polyyne

Figure 12(a) shows the finite-size behaviour of the DMC static-nucleus triplet excitonic gaps of polyyne obtained using the DFT-

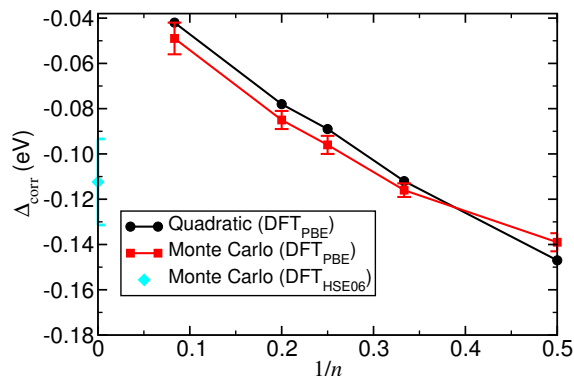


Fig. 11 DFT-PBE zero-point correction Δ_{corr} to the excitonic gaps of oligoynes as a function of the reciprocal of the number n of pairs of carbon atoms. The zero-point correction in the polyne limit was calculated by DFT-HSE06.

HSE06 and DMC ground-state geometries. In the infinite-system limit, the DMC triplet gaps with the DFT-HSE06 and DMC geometries are 2.29(7) and 3.17(7) eV, respectively. Figure 12(b) shows the static-nucleus triplet and singlet excitonic gaps and the quasiparticle gap of polyne calculated using the Ewald interaction and the DMC-optimised geometry in different supercells, together with DFT-PBE gaps. The singlet excitonic gap of polyne is slightly larger than the triplet gap. The DFT-PBE quasiparticle and excitonic gaps are calculated using the DMC-optimised geometry and Eqs. (1) and (2) at different k -point samplings (which may be unfolded to correspond to supercells of n primitive cells). The triplet excitonic gap calculated by DFT is relatively close to the DMC triplet excitonic gap, while the DFT quasiparticle gap is far too large. The DFT gap predicted by the ground-state band-structure calculation is (as expected) significantly underestimated. The fluctuations in the DFT gaps as a function of supercell size (i.e., k -point grid) are small, suggesting that single-particle errors in the DMC gaps are negligible. However, it is clear that there is a systematically varying finite-size error in the DMC gap. We have reduced the systematic finite-size errors in our DMC gaps by calculating both excitonic and quasiparticle gaps for supercells composed of 8, 10, 12, and 16 primitive cells and then extrapolating to infinite cell size using Eq. (4). The finite-size errors in the quasiparticle gaps are larger than the finite-size errors in the excitonic gaps, as discussed in Sec. 2.4. The DMC singlet and triplet excitonic gaps of polyne calculated using the DMC-relaxed geometry are 3.30(7) and 3.17(7) eV, respectively, while the DMC quasiparticle gap is 3.6(1) eV.

To estimate the unscreened exciton binding energy within the Wannier–Mott model, we have calculated the DFT-HSE06 band structure of polyne (shown in Fig. 13). In Hartree atomic units the band effective masses m_e^* and m_h^* of the electrons and holes at the X point of the Brillouin zone are given by

$$m_{e(h)}^* = \left| \frac{1}{(d^2\mathcal{E}_{C(V)})/dk^2}_X \right|, \quad (8)$$

where $\mathcal{E}_C(k)$ and $\mathcal{E}_V(k)$ are the conduction and valance bands, respectively. Numerically differentiating the DFT-HSE06 bands,

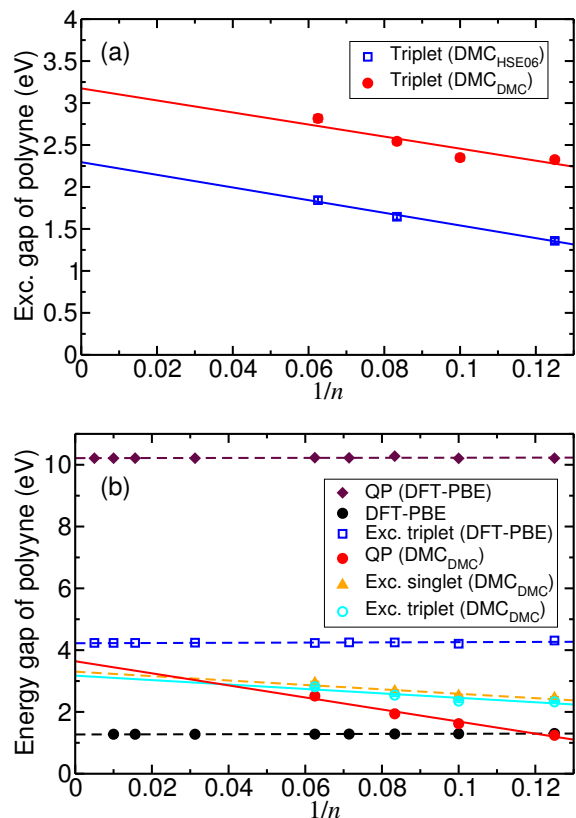


Fig. 12 (a) DMC excitonic gaps of polyne against the reciprocal of the number n of primitive cells in the supercell as calculated using the DFT-HSE06 and the DMC ground-state geometries (DMC_{HSE06} and DMC_{DMC}, respectively). (b) Quasiparticle (QP) and excitonic energy gaps of polyne against the reciprocal of the number n of primitive cells in the supercell as obtained using different methods. The results simply labelled “DFT-PBE” show the band gap obtained in a ground-state band-structure calculation. The results labelled DMC_{DMC} used the DMC ground-state geometry, whereas the results labelled DMC_{DMC(all)} used the DMC geometries for the ground state, cationic state, and anionic state of a finite cell of polyne when calculating the quasiparticle gap. The DFT calculations used the DMC geometries in the same way as the DMC calculations. At finite size the quasiparticle gap is smaller than the excitonic gap due to the introduction of a neutralising background when a charged particle is added to or removed from a periodic cell, as explained in Sec. 2.4.

we find that $m_e^* = 0.046$ a.u. and $m_h^* = 0.050$ a.u. In Hartree atomic units the exciton Bohr radius is $a_0^* = 1/\mu^*$, where $\mu^* = m_e^*m_h^*/(m_e^* + m_h^*)$ is the reduced mass of the electron–hole pair and we have assumed that the electron and hole interact via the unscreened Coulomb interaction. In this case, the exciton Bohr radius is $a_0^* = 22$ Å, which is slightly smaller than the exciton Bohr radii of about 30 Å estimated for various other 1D conjugated polymers⁷⁶, and is similar to or smaller than the lengths of the simulation cells used in our calculations (21–41 Å). Within the Wannier–Mott model, the unscreened exciton binding energy of polyne is $1R_\infty^* = \mu^*/2 = 0.3$ eV. In fact we find the DMC static-nucleus exciton binding energy to be 0.3(1) eV, which is consistent with the small measured exciton binding energies of a range of π -conjugated polymers^{77,78}.

In Fig. 14 we report the DFT-HSE06 zero-point correction to the

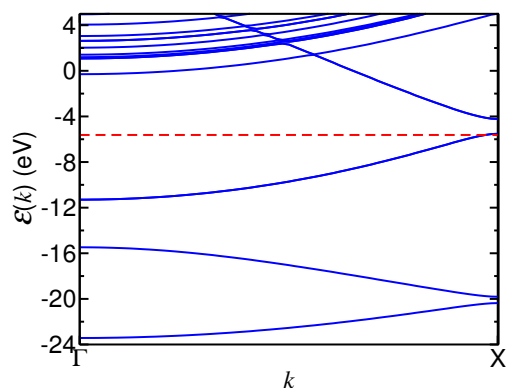


Fig. 13 DFT-HSE06 band structure of polyynes. The dashed line shows the Fermi energy.

excitonic gap of polyynes, calculated at different supercell sizes. The zero-point correction linearly extrapolated to the thermodynamic limit is $-0.11(2)$ eV. As observed for oligoynes, the vibrational correction to the gap is not as large as in benzene.

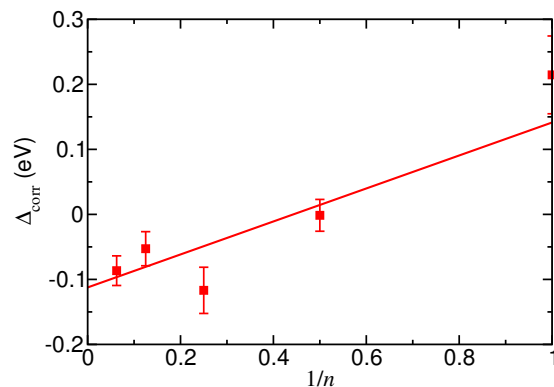


Fig. 14 DFT-HSE06 zero-point correction Δ_{corr} to the excitonic gap of polyynes against the reciprocal of the number n of primitive cells in the supercell.

In Table 4, we compare the quasiparticle and excitonic gaps of polyynes obtained by different methods. The spread of theoretical results in the literature is remarkable. The static-nucleus DMC gaps were calculated using the DMC ground-state geometry. The DMC static-nucleus singlet excitonic gap is $3.30(7)$ eV, which is slightly reduced to $3.19(7)$ eV by phonon renormalisation. By extrapolating experimental absorption gaps of oligoynes to infinite chain length, various estimates of the gap of polyynes have been made, ranging from 1.24 – 2.56 eV. These are lower than our DMC excitonic gap by 0.63 – 1.95 eV. We note that experimental gaps are strongly affected by finite chain length, solvent, and terminal groups, and that the more recent experimental results on longer oligoynes (e.g., Ref. 5) are closer to our results.

4 Conclusions

In summary we have used DMC to calculate the BLA together with the quasiparticle and excitonic gaps of hydrogen-capped oligoynes and extended polyynes. We have found that simpler levels of theory, such as DFT, do not predict either the BLA or

Table 4 Singlet excitonic gaps Δ_{exc} and quasiparticle gaps Δ_{qp} of polyynes obtained by different methods. Most of the gaps were obtained by extrapolation from a series of oligoynes molecules; the number n of pairs of carbon atoms in the largest oligoynes considered in each work is shown where known. The DFT-LDA and DFT-BLYP calculations for polyynes using periodic boundary conditions (PBC) were performed using 133 k points²⁵. Where a citation is not given in the table, the data were obtained in the present work.

Method	n	Δ_{exc} (eV)	Δ_{qp} (eV)
DFT-LDA ²⁵	PBC		0.246
DFT-LDA _x ²⁴	20		0.70
DFT-PW91 ⁷⁹	PBC		1.17
DFT-PBE	PBC		1.277
DFT-PBE1PBE ²⁵	36		1.801
DFT-B88 ²⁴	20		0.72
DFT-HF ²⁴	20		6.31
DFT-HF ²⁵	36		8.500
DFT-LHF ²⁴	20		0.92
DFT-BLYP ²⁴	20		0.72
DFT-BLYP ²⁵	PBC		0.320
DFT-B3LYP ³⁴	13		1.49
DFT-B3LYP ²⁴	20		1.50
DFT-B3LYP ²⁵	36		1.487
DFT-B3LYP ²⁶	12		1.59
DFT-KMLYP ²⁵	36		4.438
DFT-BHHLYP ²⁵	36		3.946
DFT-BHHLYP ²⁶	12		4.04
DFT-O3LYP ²⁵	36		0.895
DFT-CAM-B3LYP ²⁶	12		4.33
DFT-HSE06	PBC		1.301
GW ⁸⁰	PBC		0.407
GW ³⁸	PBC		2.15
MP2 ²⁵	20		5.541
DMC _{DMC}	PBC	3.19(7)	3.6(1)
Experiment ²³	10	2.20	
Experiment ⁷	10	2.20	
Experiment ¹⁰	12	2.18–2.36	
Experiment ³⁴	10	2.33	
Experiment ²¹	10	2.18	
Experiment ²²	12	2.16	
Experiment ¹¹	12	1.24–1.88	
Experiment ⁵	22	2.56	

the gap with quantitative accuracy. Our DMC calculations show the Peierls-induced BLA of polyynes to be $0.136(2)$ Å, which is significantly higher than DFT predictions. The DMC quasiparticle gap of extended polyynes obtained using the DMC-optimised BLA is $3.6(1)$ eV. The static-nucleus DMC singlet excitonic gap of polyynes is $3.30(7)$ eV. Vibrational contributions reduce the excitonic gap of polyynes by about 0.1 eV. The DMC-calculated zone-centre LO phonon frequency of polyynes is $2084(5)$ cm^{-1} , which is significantly higher than those obtained by DFT, but is consistent with experimental Raman measurements. Our work represents the first direct evaluation of the structural and electronic properties of extended 1D carbon chains using a high-accuracy method.

Acknowledgements

We acknowledge financial support from the UK Engineering and Physical Sciences Research Council (EPSRC). B.M. thanks Robinson College, Cambridge, and the Cambridge Philosophical Society for a Henslow Research Fellowship. This work made use of the facilities of Lancaster University's High-End Computing facility and N8 HPC provided and funded by the N8 consortium and EPSRC

(Grant No. EP/K000225/1). We acknowledge useful discussions with Viktor Zólyomi.

References

- H. W. Kroto, J. R. Heath, S. C. O'Brien, R. F. Curl and R. E. Smalley, *Astrophys. J.*, 1995, **267**, 362–367.
- W. W. Duley, *Astrophys. J.*, 2000, **10**, 362–367.
- H. W. Kroto, J. R. Heath, S. C. O'Brien, R. F. Curl and R. E. Smalley, *Nature*, 1985, **318**, 162–163.
- L. Shi, P. Rohringer, K. Suenaga, Y. Niimi, J. Kotakoski, J. C. Meyer, H. Peterlik, M. Wanko, S. Cahangirov, A. Rubio, Z. J. Lapin, L. Novotny, P. Ayala and T. Pichler, *Nat. Mater.*, 2016, advance online publication.
- W. A. Chalifoux and R. R. Tykwinski, *Nat. Chem.*, 2010, **2**, 967–972.
- R. J. Lagow, J. J. Kampa, H.-C. Wei, S. L. Battle, J. W. Genge, D. A. Laude, C. J. Harper, R. Bau, R. C. Stevens, J. F. Haw and E. Munson, *Science*, 1995, **267**, 362–367.
- T. Gibtner, F. Hampel, J.-P. Gisselbrecht and A. Hirsch, *Chem. Eur. J.*, 2002, **8**, 408–432.
- M. Tsuji, T. Tsuji, S. Kuboyama, S.-H. Yoon, Y. Korai, T. Tsujimoto, K. Kubo, A. Mori and I. Mochida, *Chem. Phys. Lett.*, 2002, **355**, 101–108.
- R. Matsutani, T. Kakimoto, K. Wada, T. Sanada, H. Tanaka and K. Kojima, *Carbon*, 2008, **46**, 1103–1106.
- W. Mohr, J. Stahl, F. Hampel and J. A. Gladysz, *Chem. Eur. J.*, 2003, **9**, 3324–3340.
- M. Samoc, G. T. Dalton, J. A. Gladysz, Q. Zheng, Y. Velkov, H. Ågren, P. Norman and M. G. Humphrey, *Inorg. Chem.*, 2008, **47**, 9946–9957.
- W. A. Chalifoux, M. J. Ferguson, R. McDonald, F. Melin, L. Echegoyen and R. R. Tykwinski, *J. Phys. Org. Chem.*, 2012, **25**, 69–76.
- Ž. Crljen and G. Baranović, *Phys. Rev. Lett.*, 2007, **98**, 116801.
- B. Standley, W. Bao, H. Zhang, J. Bruck, C. N. Lau and M. Bockrath, *Nano Lett.*, 2008, **8**, 3345–3349.
- K. H. Khoo, J. B. Neaton, Y. W. Son, M. L. Cohen and S. G. Louie, *Nano Lett.*, 2008, **8**, 2900–2905.
- P. E. Hopkins, *Appl. Phys. Lett.*, 2010, **96**, 041901.
- R. H. Baughman, *Science*, 2006, **312**, 1009–1010.
- M. Liu, V. I. Artyukhov, H. Lee, F. Xu and B. I. Yakobson, *ACS Nano*, 2013, **7**, 10075–10082.
- V. I. Artyukhov, M. Liu and B. I. Yakobson, *Nano Lett.*, 2014, **14**, 4224–4229.
- R. Peierls, *Quantum theory of solids*, Oxford University Press, Oxford, 1955, pp. 108–112.
- S. Eisler, A. D. Slepkov, E. Elliott, T. Luu, R. McDonald, F. A. Hegmann and R. R. Tykwinski, *J. Am. Chem. Soc.*, 2005, **127**, 2666–2676.
- Q. Zheng, J. C. Bohling, T. B. Peters, A. C. Frisch, F. Hampel and J. A. Gladysz, *Chem. Eur. J.*, 2006, **12**, 6486–6505.
- R. Dembinski, T. Bartik, B. Bartik, M. Jaeger and J. A. Gladysz, *J. Am. Chem. Soc.*, 2000, **122**, 810–822.
- M. Weimer, W. Hierarchy, F. D. Sala and A. Görling, *Chem. Phys.*, 2005, **309**, 77–87.
- S. Yang and M. Kertesz, *J. Phys. Chem. A*, 2006, **110**, 9771–9774.
- M. J. G. Peach, E. I. Tellgren, P. Salek, T. Helgaker and D. J. Tozer, *J. Phys. Chem. A*, 2007, **111**, 11930–11935.
- C. Zhang, Z. Cao, H. Wu and Q. Zhang, *Int. J. Quantum Chem.*, 2004, **98**, 299–308.
- A. Imamura and Y. Aoki, *Int. J. Quantum Chem.*, 2013, **113**, 423–427.
- J. P. Perdew, K. Burke and M. Ernzerhof, *Phys. Rev. Lett.*, 1996, **77**, 3865–3868.
- A. D. Becke, *J. Chem. Phys.*, 1993, **98**, 5648–5652.
- C. Lee, W. Yang and R. G. Parr, *Phys. Rev. B*, 1988, **37**, 785–789.
- J. Heyd, G. E. Scuseria and M. Ernzerhof, *J. Chem. Phys.*, 2003, **118**, 8207–8215.
- J. Heyd, G. E. Scuseria and M. Ernzerhof, *J. Chem. Phys.*, 2006, **124**, 219906.
- F. Zhuravlev and J. A. Gladysz, *Chem. A Eur. J.*, 2004, **10**, 6510–6522.
- A. Abdurahman, A. Shukla and M. Dolg, *Phys. Rev. B*, 2002, **65**, 115106.
- T. D. Poulsen, K. V. Mikkelsen, J. G. Fripiat, D. Jacquemin and B. Champagne, *J. Chem. Phys.*, 2001, **114**, 5917–5922.
- C. D. Zeinalipour-Yazdi and D. P. Pullman, *J. Phys. Chem. B*, 2008, **112**, 7377–7386.
- A. Al-Backri, V. Zólyomi and C. J. Lambert, *J. Chem. Phys.*, 2014, **140**, 104306.
- C. J. Lambert, *Chem. Soc. Rev.*, 2015, **44**, 875–888.
- D. M. Ceperley and B. J. Alder, *Phys. Rev. Lett.*, 1980, **45**, 566–569.
- W. M. C. Foulkes, L. Mitas, R. J. Needs and G. Rajagopal, *Rev. Mod. Phys.*, 2001, **73**, 33–83.
- S. J. Clark, M. D. Segall, C. J. Pickard, P. J. Hasnip, M. I. J. Probert, K. Refson and M. C. Payne, *Z. Kristallogr.*, 2005, **220**, 567.
- R. J. Needs, M. D. Towler, N. D. Drummond and P. López Ríos, *J. Phys.: Condens. Matter*, 2010, **22**, 023201.
- L. Mitáš and R. M. Martin, *Phys. Rev. Lett.*, 1994, **72**, 2438–2441.
- A. J. Williamson, R. Q. Hood, R. J. Needs and G. Rajagopal, *Phys. Rev. B*, 1998, **57**, 12140–12144.
- M. D. Towler, R. Q. Hood and R. J. Needs, *Phys. Rev. B*, 2000, **62**, 2330–2337.
- A. J. Williamson, J. C. Grossman, R. Q. Hood, A. Puzder and G. Galli, *Phys. Rev. Lett.*, 2002, **89**, 196803.
- N. D. Drummond, A. J. Williamson, R. J. Needs and G. Galli, *Phys. Rev. Lett.*, 2005, **95**, 096801.
- T. Xie, J. Bowman, J. W. Duff, M. Braunstein and B. Ramachandran, *J. Chem. Phys.*, 2005, **122**, 014301.
- J. R. Trail and R. J. Needs, *J. Chem. Phys.*, 2005, **122**, 174109.
- D. Alfè and M. J. Gillan, *Phys. Rev. B*, 2004, **70**, 161101.
- M. P. Nightingale and V. Melik-Alaverdian, *Phys. Rev. Lett.*,

- 2001, **87**, 043401.
- 53 J. Toulouse and C. J. Umrigar, *J. Chem. Phys.*, 2007, **126**, 084102.
- 54 C. J. Umrigar, J. Toulouse, C. Filippi, S. Sorella and R. G. Hennig, *Phys. Rev. Lett.*, 2007, **98**, 110201.
- 55 C. J. Umrigar, K. G. Wilson and J. W. Wilkins, *Phys. Rev. Lett.*, 1988, **60**, 1719–1722.
- 56 N. D. Drummond and R. J. Needs, *Phys. Rev. B*, 2005, **72**, 085124.
- 57 J. B. Anderson, *J. Chem. Phys.*, 1976, **65**, 4121–4127.
- 58 R. M. Lee and N. D. Drummond, *Phys. Rev. B*, 2011, **83**, 245114.
- 59 F. Giustino, S. G. Louie and M. L. Cohen, *Phys. Rev. Lett.*, 2010, **105**, 265501.
- 60 B. Monserrat and R. J. Needs, *Phys. Rev. B*, 2014, **89**, 214304.
- 61 G. Antonius, S. Poncé, P. Boulanger, M. Côté and X. Gonze, *Phys. Rev. Lett.*, 2014, **112**, 215501.
- 62 C. E. Patrick and F. Giustino, *Nat. Commun.*, 2013, **4**, 2006.
- 63 K. Kunc and R. M. Martin, *Phys. Rev. Lett.*, 1982, **48**, 406–409.
- 64 B. Monserrat, N. D. Drummond, C. J. Pickard and R. J. Needs, *Phys. Rev. Lett.*, 2014, **112**, 055504.
- 65 P. B. Allen and V. Heine, *J. Phys. C*, 1976, **9**, 2305.
- 66 G. Nemeth, H. Selzle and E. Schlag, *Chem. Phys. Lett.*, 1993, **215**, 151–155.
- 67 J. P. Doering, *J. Chem. Phys.*, 1969, **51**, 2866–2870.
- 68 A. Hiraya and K. Shobatake, *J. Chem. Phys.*, 1991, **94**, 7700.
- 69 C. E. Patrick and F. Giustino, *J. Phys.: Condens. Matter*, 2014, **26**, 365503.
- 70 T. Pino, H. Ding, F. Güthe and J. P. Maier, *J. Chem. Phys.*, 2001, **114**, 2208–2212.
- 71 U. Mölder, P. Burk and I. A. Koppel, *Int. J. Quantum Chem.*, 2001, **82**, 73–85.
- 72 S. Cahangirov, M. Topsakal and S. Ciraci, *Phys. Rev. B*, 2010, **82**, 195444.
- 73 A. Milani, M. Tommasini, D. Fazzi, C. Castiglioni, M. D. Zoppo and G. Zerbi, *J. Raman Spectrosc.*, 2008, **39**, 164–168.
- 74 M. Wanko, S. Cahangirov, L. Shi, P. Rohringer, Z. J. Lapin, L. Novotny, P. Ayala, T. Pichler and A. Rubio, *arXiv: 1604.00483*, 2016.
- 75 N. R. Agarwal, A. Lucotti, D. Fazzi, M. Tommasini, C. Castiglioni, W. Chalifoux and R. R. Tykwinski, *J. Raman Spectrosc.*, 2013, **44**, 1398–1410.
- 76 A. J. Heeger, *Rev. Mod. Phys.*, 2001, **73**, 681–700.
- 77 M. Knupfer, *App. Phys. A*, 2003, **77**, 623–626.
- 78 D. Moses, J. Wang, A. J. Heeger, N. Kirova and S. Brazovski, *PNAS*, 2001, **98**, 13496–13500.
- 79 Y. Shujuan, Z. Chenggang, W. Jinping, L. Jiaye, H. Bo and C. Hansong, *Int. J. Quantum Chem.*, 2008, **108**, 1565–1571.
- 80 O. Cretu, A. R. Botello-Mendez, I. Janowska, C. Pham-Huu, J.-C. Charlier and F. Banhart, *Nano Lett.*, 2013, **13**, 3487–3493.